[7]G. W. Greenlees, C. H. Poppe, J. A. Sievers, and D. L. Watson, Phys. Rev. C 3, 1231 (1971).
[8]M. Q. Makino, C. N. Waddell, and R. M. Eisberg, Nucl. Instr. Methods 60, 109 (1968); J. J. Kraushaar, R. A. Ristinen, and R. Smythe, Phys. Letters 25B, 13 (1967).
[9]R. N. Boyd, J. Fenton, M. Williams, T. Kruse, and W. Savin, Nucl. Phys. A162, 497 (1971).
[10]J. F. Dicello, G. Igo, and M. L. Roush, Phys. Rev. 157, 1001 (1967); R. E. Pollock, Ph.D. thesis, Princeton University, 1962 (unpublished).
[11]F. D. Becchetti, Jr., M.S. thesis, University of Minnesota, 1968 (unpublished).

PHYSICAL REVIEW C VOLUME 5, NUMBER 3 MARCH 1972

Experimental 0_2^+ (2.12 MeV) → 2_1^+ (1.46 MeV) $B(E2)$ Strength and Pairing-Vibration Calculations in ^{40}Ar†

S. H. Henson,* S. Cochavi,‡ D. B. Fossan, and J. D. Vergados
State University of New York, Stony Brook, New York 11790
(Received 6 August 1971)

The lifetime of the 2.12-MeV 0_2^+ state in ^{40}Ar has been measured by a p-γ delayed-coincidence technique. This state was populated by the (p, p') reaction with 5.3-MeV protons bombarding an Ar gas target. A mean lifetime of $\tau = 150 \pm 20$ psec was obtained for the 0_2^+ state. This lifetime implies for the $0_2^+ \rightarrow 2_1^+$ transition $B(E2) = 42.9 \pm 5.7\ e^2\,\mathrm{F}^4$. Pairing-vibration model calculations for ^{40}Ar were made using experimental information regarding energies and $B(E2)$ strengths for the three lowest levels of both ^{42}Ca and ^{38}Ar. Three kinds of interaction were considered: first, no interaction; second, a phenomenological quadrupole-quadrupole interaction; and third, the Kuo-Brown bare G matrix elements. None of these calculations can accurately describe both the energy spectrum and the $E2$ transition strengths in ^{40}Ar. This result may be an indication of the inadequacy of the pairing-vibration model for ^{40}Ar.

INTRODUCTION

Previous studies[1,2] have indicated limited success for the pairing-vibration model in certain nuclear regions. T. T. S. Kuo and one of the authors (J.D.V.) have suggested an experiment involving the measurement of electromagnetic transition strengths in ^{40}Ar as a test of the applicability of the pairing-vibration model in ^{40}Ar. With this model, states in ^{40}Ar are constructed from the coupling of low-lying two-particle phonons to low-lying two-hole phonons; thus, the 0_1^+ (first 0^+) ground state of ^{40}Ar might be described as a product of the two-particle phonon representing the ground state of ^{42}Ca and the two-hole ground-state phonon of ^{38}Ar. Similar phonon structures might describe the 2_1^+ state at 1.46 MeV and the 0_2^+ (second 0^+) state at 2.12 MeV in ^{40}Ar; these states would also involve the two-particle and two-hole phonon representations of the 2_1^+ states in ^{38}Ar and ^{42}Ca. The inclusion of phonons representing the 0_2^+ states in ^{38}Ar and ^{42}Ca would add an additional degree of flexibility.

One test of the validity of this model for ^{40}Ar can be made by a comparison of the measured $0_2^+ \rightarrow 2_1^+$ and $2_1^+ \rightarrow 0_1^+$ $E2$ transition strengths with those expected on the basis of this model, which can be calculated from known lifetimes[3-5] in ^{38}Ar and ^{42}Ca. Since the ^{40}Ar $2_1^+ \rightarrow 0_1^+$ transition strength has been measured,[6,7] the only remaining measurement for this test is that of the lifetime of the 0_2^+ level at 2.12 MeV in ^{40}Ar which yields the $0_2^+ \rightarrow 2_1^+$ $E2$ strength.

The purpose of the present study is thus to measure the lifetime of the 0_2^+ state in ^{40}Ar in order to complete this test of the applicability of the pairing-vibration model to ^{40}Ar. The experiment was performed with an electronic-timing technique in conjunction with the reaction $^{40}\mathrm{Ar}(p, p'\gamma)^{40}\mathrm{Ar}$.

EXPERIMENTAL TECHNIQUE

Two reactions, $^{37}\mathrm{Cl}(\alpha, p)^{40}\mathrm{Ar}$ and $^{40}\mathrm{Ar}(p, p')^{40}\mathrm{Ar}$, were considered as a means of populating the 0_2^+ state at 2.12 MeV in ^{40}Ar. The low-lying level scheme[8,9] for ^{40}Ar is shown in Fig. 1. As an ^{40}Ar target requires a gas cell, the reaction $^{37}\mathrm{Cl}(\alpha, p)^{40}\mathrm{Ar}$ was tried first. A 400-μg/cm^2 $BaCl_2$ target isotopically enriched in ^{37}Cl was prepared by evaporation onto a thin C foil. The proton spectra from the reaction $^{37}\mathrm{Cl}(\alpha, p)^{40}\mathrm{Ar}$ for several angles from 30 to 90° were studied with a solid-state detector over an energy range of $E_\alpha = 6$–12 MeV. The yield to the 0_2^+ state in ^{40}Ar, although nonzero, was sufficiently weak in the region studied as to make a delayed-coincidence timing measurement impossible.

As a result of the weak yield from the reaction

$^{37}Cl(\alpha, p)^{40}Ar$, the reaction $^{40}Ar(p, p')^{40}Ar$ with a gas target was employed for this experiment. The gas cell designed for this measurement is shown in Fig. 2. Entrance and exit windows were of 0.05-mil Ni foil, and about 0.5 atm (~400 $\mu g/cm^2$) of natural Ar gas was used in the cell. The active volume of the gas cell was defined by collimation to minimize geometric transit-time contributions to the time resolution.

An excitation study of the reaction $^{40}Ar(p, p')^{40}Ar$ was made from 5- to 6-MeV proton energy in steps of 100 keV by observing the proton spectra at 120° in a solid-state detector. A proton energy of $E_p = 5.3$ MeV was chosen for optimum yield to the 0_2^+ 2.12-MeV state in ^{40}Ar. Figure 3 shows a semilog plot of the proton spectrum at $\theta = 120°$ from the reaction $^{40}Ar(p, p')^{40}Ar$ for $E_p = 5.3$ MeV. Proton groups from the ground state and the first four excited states in ^{40}Ar were observed along with gas contaminant elastic groups. The broad peak in the group of elastic contaminants results from the Ne isotopes and possibly a small amount of F, while the next three narrow elastic peaks are from O, N, and C. The shoulder to the left of the ^{40}Ar 2.12-MeV peak has the correct energy for elastic scattering from a He contaminant. For these experimental conditions, the ^{40}Ar groups are well separated as shown in Fig. 3; the cross section to the 2_1^+ 1.46-MeV state is about twice that of the 0_2^+ 2.12-MeV state. The small shoulder to the right of the ^{40}Ar 2.12-MeV peak with a relative amplitude of about 2% is believed to be the inelastic peak from the 1.63-MeV first excited state of ^{20}Ne which results from the Ne contaminant. In the timing measurements with the 2.12-MeV proton group, this small shoulder was excluded by pulse-height selection. Furthermore, the 1.63-MeV ^{20}Ne state has a mean lifetime of 0.8 psec which, if included to some small extent, would make only a prompt contribution.

The lifetime of the 0_2^+ 2.12-MeV state was obtained from a measurement of the distribution of time delays between formation and decay of the state. The time of formation was determined by the detection of the 0_2^+ proton group from the reaction $^{40}Ar(p, p')^{40}Ar$ in the solid-state detector, while the time of decay was marked by the detection of the 1.46-MeV γ rays in a plastic scintillator. The 0_2^+ 2.12-MeV state decays by a 660-keV γ ray to the 2_1^+ 1.46-MeV state; the mean lifetime of the 2_1^+ 1.46-MeV state is 1.2 ± 0.3 psec.[6] Since

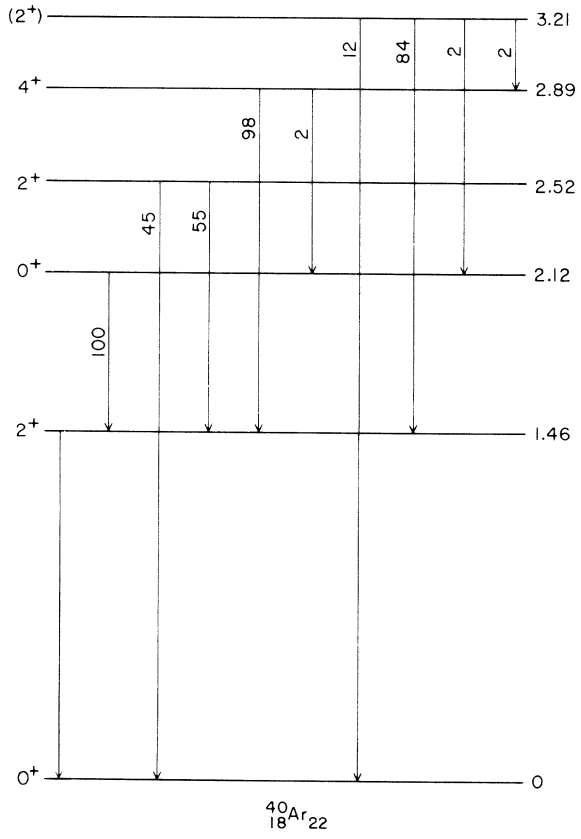

FIG. 1. Levels in ^{40}Ar below 3.3 MeV. The level scheme, spin-parity parameters, and branching ratios are consistent with those given in Refs. 6 and 7.

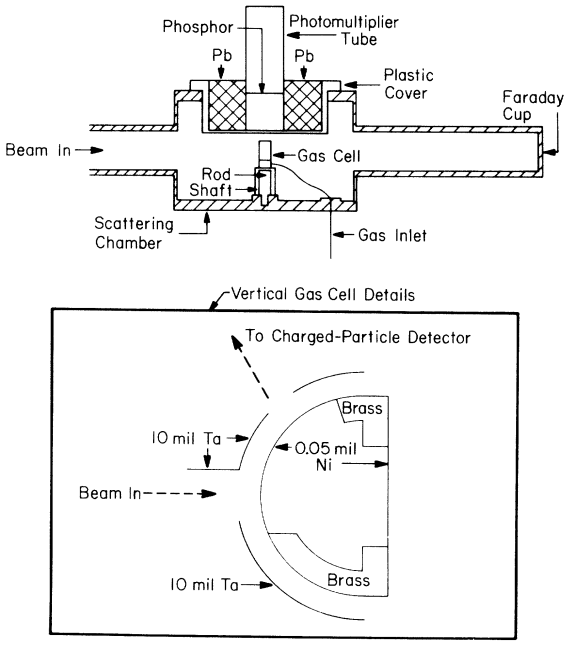

FIG. 2. A schematic diagram of the gas cell and of the scattering chamber used for the particle-γ delayed-coincidence measurements. The charged-particle detector, not shown, is in the plane perpendicular to the γ detector and the beam.

the 2.12-MeV state is estimated to have a mean lifetime greater than 100 psec, the higher-energy 1.46-MeV $2_1^+ \rightarrow 0_1^+$ γ decay can be used to mark the decay of the 0_2^+ 2.12-MeV state. Better time resolution is obtainable with the higher-energy γ transition, and, as discussed later, this transition allows a simultaneous measurement of the prompt resolution function (PRF). The time-delay pulses were produced in a time-to-amplitude converter (TAC) in the usual fast-slow coincidence arrangement.[10]

The protons were detected in a surface-barrier solid-state detector of 400-μ thickness and 50-mm^2 area which was positioned at 120° to the beam direction at 3 cm from the gas cell. The detector was rotated about its axis by 45°, achieving an effective thickness of 570 μ. This detector arrangement stopped protons with energies up to the elastic group, and resulted in improved collection times because a larger amount of the energy is deposited near the surface. The γ detector was an NE102 (Nuclear Enterprises) plastic scintillator coupled to an XP1020 (Amperex) photomultiplier tube; its axis was placed perpendicular to the reaction plane defined by the proton beam and proton detector (see Fig. 2). The γ detector was shielded with 3 mm of lead to attenuate low-energy γ rays.

Figure 4 shows a schematic diagram of the experimental electronics. From the γ-ray pulse-height distribution, the upper portion of the Compton edge of the 1.46-MeV γ ray was accepted in the pulse-height window of single-channel analyzer (SCA) 1. SCA 2 accepted only the 2_1^+ 1.46-MeV proton group in its pulse-height window, and SCA 3 the 0_2^+ 2.12-MeV proton group. Since the lifetime of the 1.46-MeV state is known to be short relative to the time resolution of this system, the time-delay spectrum associated with the 1.46-MeV proton group represents the PRF. Thus, the 2.12-MeV state time-delay spectrum and the PRF were measured simultaneously.[10]

EXPERIMENTAL RESULTS

The initial data for the time-delay distribution of the 0_2^+ 2.12-MeV state in ^{40}Ar indicated that the lifetime slope of the decay curve was only slightly larger than the lower limit of the experiment, namely, the slope of the PRF. For lifetimes in this limiting region, both the decay curve and the corresponding PRF have to be measured with considerable precision in order to obtain a lifetime with reasonable accuracy. Thus, the simultaneous measurements of the PRF along with the decay curve, as discussed in the previous section, were essential for this experiment.

Three different measurements of the 0_2^+ state decay curve were made; the results are listed in Table I. The compromise between time resolution and statistics was changed for the different runs by varying the ^{40}Ar gas pressure and the accepted dynamic range of the γ-ray Compton spectrum. It was necessary to show that the slope of the PRF was less than that of the decay curve, and also the decay curve slope had to be deter-

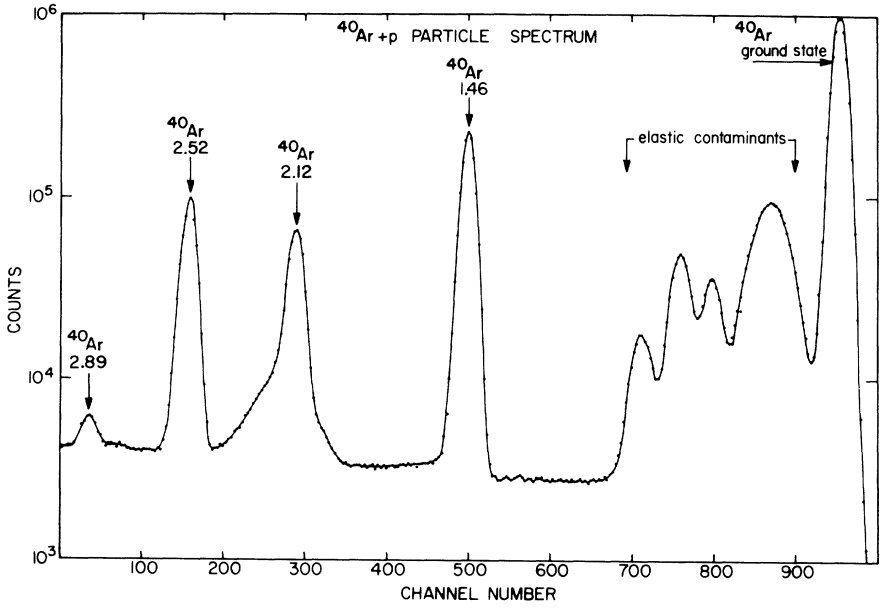

FIG. 3. Charged-particle spectrum at 120° for $E_p = 5.3$ MeV from ^{40}Ar + p.

mined accurately. For run No. 2 (~20% γ window), the time resolution was favored in the compromise, while for run No. 3 (~30% γ window), the coincidence yield and therefore the statistics were improved with a slight sacrifice in the time resolution.

The filled circles in Figs. 5 and 6 show the time-delay spectrum for the 0_2^+ 2.12-MeV state, for run Nos. 2 and 3, respectively, while the open circles show the corresponding PRF obtained from the 2_1^+ proton group. Background subtraction and a normalization have been performed. A relative shift in the position of the decay curve and the PRF also has been made. This shift, which amounted to approximately 400 psec, was based both on the knowledge that the maximum of the decay curve should intersect the PRF, and on an estimate of the difference in proton flight times and the time walk at the discriminator. Although the rise time of the proton pulses associated with the detector and the time pick-off (TPO) has been studied with prompt inelastic scattering groups for a common γ window, the estimate of the shift including both the time walk and the difference in flight times is not believed to be any better than ±50 psec. The data obtained in run No. 1 are not shown. The shapes of the prompt resolution functions appearing in Figs. 5 and 6 are not Gaussian, but show an asymmetry to the right. To assess the minimum possible lifetime measurable with the PRF, the right slope of the PRF was least-squares fitted to an exponential. For each run, fits were made to different portions of the PRF to achieve the most appropriate slope. Using the data region shown with error bars, the time required for this slope to fall by a factor of e is listed in the second column of Table I; this time is analogous to the minimum obtainable τ. The PRF τ_{min} for run No. 2 was 112 ± 9 psec and the corresponding full width at half maximum (FWHM) was 450 psec; these values do not represent the minimum capabilities of the electronic instrumentation, but rather indicate the geometric transit-time limitations of the gas target. The uncertainties for each run are indicated in Table I; these were estimated from the statistics and the quality of the fits.

To demonstrate that the decay curve of the 0_2^+ state is different from the PRF, similar time regions of the decay curves were fitted to an exponential. The time required for the logarithmic slope of the 0_2^+ decay curve to fall by a factor of e is given in the third column of Table I. The average slope of the decay curve for the three runs is 177 psec. The above results show with statistical significance that the right slope of the 0_2^+ decay curve falls more slowly with time than the right slope of the PRF for all three runs.

The time required for the fitted slope of the 0_2^+ decay curve to fall by a factor of e is not directly the mean life of the state, since several of the experimental points used in the fits do not receive contributions from the entire PRF, as can be seen in Figs. 5 and 6. Methods of lifetime extraction appropriate to this situation have been described by Newton.[11] The large-time region of the decay curves were first fitted to exponentials using only data points to the right of an initial channel for which the PRF fit was less than ~10% of the decay curve. Additional fits were made using more data points up to an initial channel for which the PRF amounted to ~20%. For most of these fits, the effect of the PRF is very small, as given by Eq. (4) of Newton. The integral expression, Eq. (5) of Newton, was secondly used for several larger regions of the decay curve to determine the mean

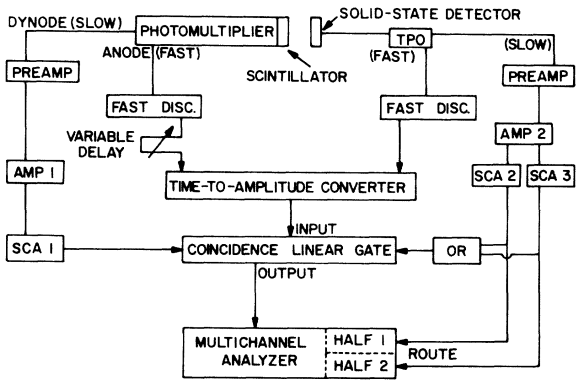

FIG. 4. A schematic diagram of the experimental electronics for charged-particle–γ delayed-coincidence measurements.

TABLE I. The second and third columns list the logarithmic slopes in terms of the time to fall by a factor of e; these slopes represent exponential fits of the PRF and the decay curve for the 0_2^+ 2.12-MeV state in ^{40}Ar. The fourth column lists the actual mean life of the 0_2^+ state deduced from expressions in Ref. 11. The final value of 150 ± 20 psec for the mean life is a weighted average of the above three values. The over-all uncertainty is based on the estimated uncertainties in the three runs which include statistical uncertainties, possible systematic errors, and time-calibration uncertainties. All time values are given in units of psec.

Run No.	PRF slope	Decay-curve slope	Mean life (psec)
1	111 ± 12	172 ± 18	145
2	112 ± 9	169 ± 13	142 } 150 ± 20
3	134 ± 6	190 ± 9	157

lifetime with smaller statistical uncertainties; for these calculations, however, the uncertainty in the time position of the PRF is more important. Thirdly, the analysis was repeated using different PRF relative-time positions over a range of ~±50 psec. The averages of the sequence of mean-lifetime values generated by this analysis are listed in the fourth column of Table I. The final value of 150 ± 20 psec for the mean life of the 0_2^+ state in ^{40}Ar is a weighted average of the above three values. The uncertainty listed of about ±15% includes all but the extreme mean-lifetime values of the above analysis; this conservative error estimate incorporates the concern over possible systematic errors in the analysis such as for the PRF time position. The statistical uncertainties for a fixed PRF position, which equals about ±6%, is a small part of the total uncertainty, as is a 2% time-calibration uncertainty. The time difference between the centroids of the decay curve and the PRF is consistent within uncertainties with the final mean-lifetime value. This lifetime yields a reduced $E2$ transition strength for the $0_2^+ \rightarrow 2_1^+$ transition in ^{40}Ar of $B(E2) = 42.9 \pm 5.7\ e^2\,\mathrm{F}^4$.

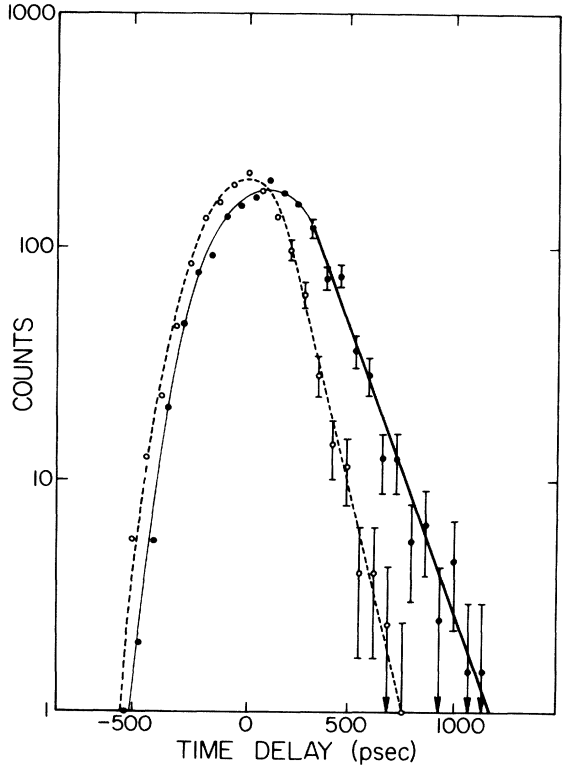

FIG. 5. The experimental decay curve obtained in run No. 2 for the 0^+ 2.12-MeV state in ^{40}Ar is shown in filled circles and the solid line. The right slope of the decay curve falls by a factor of e in 169 psec. The PRF is shown with open circles and the dashed line; the right slope of the PRF falls by a factor of e in 112 psec. A time shift and a normalization of the PRF have been made.

DISCUSSION

The nucleus ^{40}Ar in expected to be described rather well within the framework of the shell model with two neutrons in the $1f$-$2p$ shell and two proton holes in the $1d$-$2s$ shell. Such a calculation[2] has in fact been performed and was found able to reproduce rather well the low-lying portion of the spectrum of ^{40}Ar with the exception of the 0_2^+ state, which was found to lie 1.5 MeV higher than the experimental value. In addition the applicability of the pairing-vibration model was tested in this case and the results were negative. However, since the structure of the two-particle phonon and the two-hole phonon was restricted because of the model space used, the pairing-vibration model cannot be completely ruled out as a useful means of understanding this nuclear system.

In the present investigation, an attempt will be made to explain the experimental situation in ^{40}Ar with the pairing-vibration model treating the phonons involved phenomenologically. This seems to

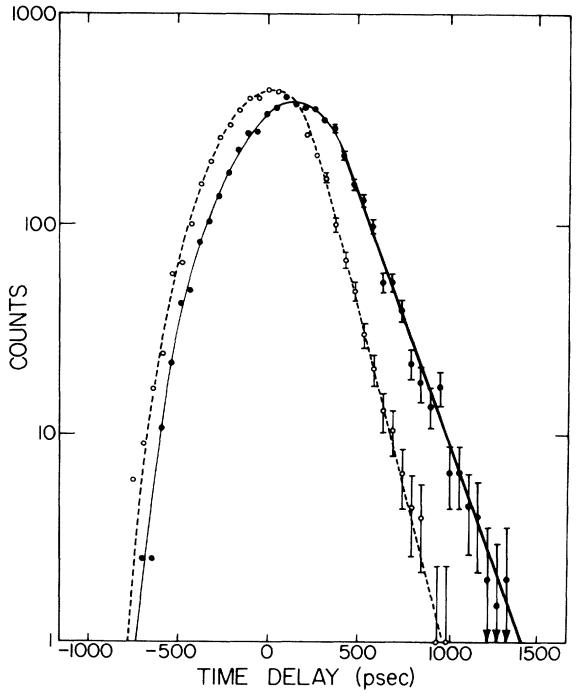

FIG. 6. The experimental decay curve obtained in run No. 3 for the 0^+ 2.12-MeV state in ^{40}Ar is shown with filled circles and the solid line. The right slope of the decay curve falls by a factor of e in 190 psec. The PRF is shown with open circles and the dashed line; the right slope of the PRF falls to $1/e$ of its value in 134 psec. A time shift and a normalization of the PRF have been made.

TABLE II. Experimental $B(E2)$ values for transitions in ^{40}Ar, ^{42}Ca, and ^{38}Ar.

Nucleus	Transitions (MeV)	$J^\pi_i \rightarrow J^\pi_f$	Experimental $B(E2)$ (e^2 F^4)
^{40}Ar	2.12 → 1.46	$0^+_2 \rightarrow 2^+_1$	42.9 ± 5.7 [a]
^{40}Ar	1.46 → 0	$2^+_1 \rightarrow 0^+_1$	105 ± 26 [b]
^{42}Ca	1.84 → 1.52	$0^+_2(+) \rightarrow 2^+_1(+)$	556 ± 34 [c]
^{42}Ca	1.52 → 0	$2^+_1(+) \rightarrow 0^+_1(+)$	74 ± 17 [d]
^{38}Ar	3.38 → 2.17	$0^+_2(-) \rightarrow 2^+_1(-)$	46 ± 26 [e]
^{38}Ar	2.17 → 0	$2^+_1(-) \rightarrow 0^+_1(-)$	32 ± 4 [e]

[a] Present work.

[b] Taken from Ref. 6. The value from Ref. 7 is $B(E2) = 50 \pm 50$ e^2 F^4; it has not been averaged with previous results because of the large uncertainties.

[c] Taken from Ref. 5.

[d] Taken from Ref. 4. The resonance fluorescence value of Metzger and Tandon has been used; the Doppler-shift attenuation method result 62 ± 7 e^2 F^4 of Kossler *et al.* is consistent with this value.

[e] Taken from Ref. 3.

be the most appropriate way, since the excited states of ^{42}Ca are known to have large deformations.[12,13] On the basis of the pairing-vibration model it is expected that the nucleus ^{40}Ar can be understood in terms of the known properties of ^{42}Ca and ^{38}Ar. Experimental $B(E2)$ values of transitions in ^{38}Ar, ^{42}Ca, and ^{40}Ar are summarized in Table II. One starts from the two-hole phonons $0^+_1(-)$, $2^+_1(-)$ that describe the ground and first excited states of ^{38}Ar and the two-particle phonons $0^+_1(+)$, $2^+_1(+)$ that describe the ground and first excited states of ^{42}Ca. The following states of ^{40}Ar can be constructed:

(a) 0^+ states:

$$|1\rangle = |0^+_1(+)0^+_1(-)\rangle ,$$

and

$$|2\rangle = |2^+_1(+)2^+_1(-)\rangle ,$$

with energies 0 and 3.70 MeV, respectively.

(b) 2^+ states:

$$|1\rangle = \frac{1}{\sqrt{2}} |0^+_1(+)2^+_1(-) - 2^+_1(+)0^+_1(-)\rangle ,$$

$$|2\rangle = \frac{1}{\sqrt{2}} |0^+_1(+)2^+_1(-) + 2^+_1(+)0^+_1(-)\rangle ,$$

and

$$|3\rangle = |2_1(+)2_1(-)\rangle ,$$

with energies 1.85, 1.85, and 3.70 MeV, respectively. For comparison purposes we identify the $|1\rangle$ and $|2\rangle$ 0^+ states as the 0^+_1 and 0^+_2 states, and the $|1\rangle$, $|2\rangle$, and $|3\rangle$ 2^+ states as the 2^+_1, 2^+_2, and 2^+_3 states, respectively, in ^{40}Ar. The above energies for the 0^+ and 2^+ states which are obtained from the spectrum and binding energies of ^{38}Ar and ^{42}Ca are inconsistent with the experimental energies in ^{40}Ar. Although the calculated energies are not in good agreement with experiment, a comparison of experimental and calculated $E2$ strengths is of interest. From the known $B(E2; 2^+_1(+) \rightarrow 0^+_1(+)) = 74 \pm 17$ e^2 F^4 and $B(E2; 2^+_1(-) \rightarrow 0^+_1(-)) = 32 \pm 4$ e^2 F^4 (see Table II), one finds $B(E2; 2^+_1 \rightarrow 0^+_1) = B(E2; 0^+_2 \rightarrow 2^+_1) = 102$ e^2 F^4. Theoretical $B(E2)$ values for ^{40}Ar are listed in Table III. The above result agrees with the experimental value for the $2^+_1 \rightarrow 0^+_1$ transition within the experimental uncertainties, but not with the $0^+_2 \rightarrow 2^+_1$ experimental $B(E2)$. Mixing of the above states is not likely to improve the situation. The nuclear interaction has a rather strong quadrupole-quadrupole component and one expects a strong coupling, e.g., between the 0^+_1 and 0^+_2 states, which will result in a still larger energy difference between the two 0^+ states. It seems imperative, therefore, to expand the above model space. This model and subsequent expansions yield small values for the $B(E2; 2^+_2 \rightarrow 0^+_1)$ and

TABLE III. Comparison of theoretical $B(E2)$ (e^2 F^4) values for $0^+_2 \rightarrow 2^+_1$ and $2^+_1 \rightarrow 0^+_1$ transitions in ^{40}Ar from the various calculations described in the text.

$J_i \rightarrow J_f$	$0^+_1(\pm)$, $2^+_1(\pm)$ phonons	$0^+_1(\pm)$, $2^+_1(\pm)$, $0^+_2(\pm)$ phonons			
		No mixing	Interaction A	Interaction B	Experimental
$0^+_2 \rightarrow 2^+_1$	102	556	388	288	42.9 ± 5.7
$2^+_1 \rightarrow 0^+_1$	102	74	88	152	105 ± 26

$B(E2; 2_3^+ \rightarrow 0_1^+)$ which are consistent with experimental results.[8]

The above model space can be extended by noticing that there exist second 0^+ states for both ^{38}Ar$[0_2^+(-)]$ and ^{42}Ca$[0_2^+(+)]$ which lie low in energy. Hence the following basis is constructed:
(a) 0^+ states:

$$|1\rangle = |0_1^+(+)0_1^+(-)\rangle, \quad |2\rangle = |0_2^+(+)0_1^+(-)\rangle,$$

$$|3\rangle = |0_1^+(+)0_2^+(-)\rangle, \quad |4\rangle = |2_1^+(+)2_1(-)\rangle,$$

and

$$|5\rangle = |0_2^+(+)0_2^+(-)\rangle,$$

with unperturbed energies 0., 1.84, 3.37, 3.70, and 5.21 MeV, respectively.
(b) 2^+ states:

$$|1\rangle = |2_1(+)0_1(-)\rangle, \quad |2\rangle = |0_1^+(+)2_1^+(-)\rangle,$$

$$|3\rangle = |2_1^+(+)2_1^+(-)\rangle, \quad |4\rangle = |0_2^+(+)2_1(-)\rangle,$$

and

$$|5\rangle = |2_1^+(+)0_2^+(-)\rangle,$$

with unperturbed energies 1.53, 2.17, 3.70, 4.01, and 4.90 MeV, respectively.

If one identifies the lowest of the above states with the known experimental energy levels, the agreement with experiment as far as energies are concerned has substantially improved. However,

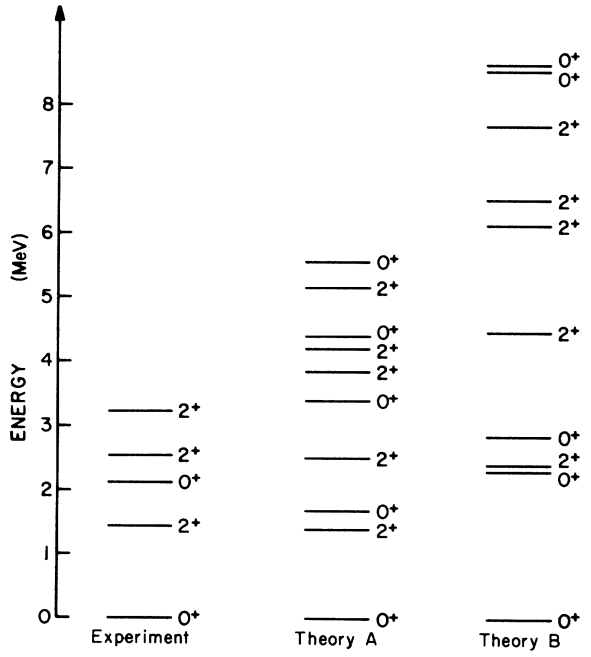

FIG. 7. Experimental and theoretical predicted energy levels in ^{40}Ar. In theory case A the phenomenological interaction described in the text was used. In case B a realistic nucleon-nucleon interaction was used.

TABLE IV. Hamiltonian matrices using $V = KQ \cdot Q$ ($K = 0.0069$) (basis states defined in text).

|1⟩	|2⟩	|3⟩	|4⟩	|5⟩	
		0^+ states			
0	0	0.749 04	0.	0.	|1⟩
	1.84	−0.919 91	0.	0.	|2⟩
		3.70	−0.402 64	0.494 49	|3⟩
			3.37	0.	|4⟩
				5.21	|5⟩
		2^+ states			
2.27	0	0.334 98	0.	−0.180 68	|1⟩
	401	−0.411 40	0.	0.221 15	|2⟩
		1.53	0.	0.	|3⟩
			3.70	0.145 46	|4⟩
				4.90	|5⟩

from the known $B(E2; 0_2^+(+) \rightarrow 2_1^+(+)) = 556 \pm 34\ e^2\,F^4$ and $B(E2; 0_2^+(-) \rightarrow 2_1^+(-)) = 46 \pm 26\ e^2\,F^4$, we get for the $B(E2)$ transitions in ^{40}Ar: $B(E2; 2_1^+ \rightarrow 0_1^+) = 74\ e^2\,F^4$, and $B(E2; 0_2^+ \rightarrow 2_1^+) = 556\ e^2\,F^4$. The predicted values are not in good agreement with experiment, as seen in Table III. In order to improve the calculation, mixing of the above states is allowed via the residual interaction. Two approaches, A and B, were adopted to that effect.

Calculation A. A phenomenological interaction of the form $KQ \cdot Q$ was considered (quadrupole-quadrupole interaction). In order to evaluate the matrix elements of this interaction we assumed that the quadrupole moment is the same as the electric quadrupole moment (i.e., the effective charges for both neutrons and protons were assumed to be equal to e). Then the matrix elements $\langle J_i(+) \| E2 \| J_j(+) \rangle$ and $\langle J_i(-) \| E2 \| J_j(-) \rangle$ can be determined from the known $B(E2)$ values (see Table II) and quadrupole moments. The relative signs were determined by using the shell-model

TABLE V. Hamiltonian matrices using realistic two-body interaction (basis states defined in text).

|1⟩	|2⟩	|3⟩	|4⟩	|5⟩	
		0^+ states			
0	−0.48668	3.775 99	−0.418 05	0.226 27	|1⟩
	−0.08	−0.072 87	0.226 26	0.508 81	|2⟩
		3.70	0.004 67	−0.019 42	|3⟩
			3.37	0.613 35	|4⟩
				5.21	|5⟩
		2^+ states			
2.27	−0.52210	1.690 47	0.479 31	0.004 76	|1⟩
	2.12	−0.067 32	0.019 06	0.013 74	|2⟩
		1.60	−0.652 50	−0.424 90	|3⟩
			3.70	0.073 06	|4⟩
				8.17	|5⟩

two-particle and two-hole wave functions. The quadrupole moment of the $2_1^+(-)$ state has recently[14] been measured and found to be 0.137 e^2 F^4. This small value is consistent with the shell-model prediction, since this state is predominantly a $d_{3/2}^{-2}$ configuration ($\langle d_{3/2}^{-2} \| E2 \| d_{3/2}^{-2} \rangle = 0$). The quadrupole moment of the $2_1^+(+)$ state is not known experimentally; it was determined from the known $B(E2; 2_1^+(+) \rightarrow 0_1^+(+))$ and the ratio $\langle 2_1^+(+) \| E2 \| 0_1^+(+) \rangle / \langle 2_1^+(+) \| E2 \| 2_1^+(+) \rangle$. The latter was determined by assuming pure $f_{7/2}^2$ for the $2_1^+(+)$ and $0_1^+(+)$ states. The parameter K was chosen so that the energy difference $E(2_2^+) - E(2_1^+)$ is equal to the experimental energy separation of these states.

The energy matrices appear in Table IV and the resulting energy spectrum appears in Fig. 7, theory A. The predicted energy levels are in fairly good agreement with experiment. The coupling is not very strong and the eigenstates remain relatively pure.

The calculated quadrupole transitions of interest are (see Table III): $B(E2; 2_1^+ \rightarrow 0_1^+) = 88$ e^2 F^4, and $B(E2; 0_2^+ \rightarrow 2_1^+) = 388$ e^2 F^4. The respective ^{40}Ar experimental values are 105 and 42.9 e^2 F^4 as seen in Table II. The theoretical $B(E2; 0_2^+ \rightarrow 2_1^+)$ was somewhat reduced but it is still about 9 times larger than experiment.

Calculation B. Realistic two-body interactions were considered as the second approach. The Kuo-Brown[15] bare G matrix elements derived from the Hamada-Johnson potential were used. The method of calculation was the same as in Ref. 2 with the modification that the experimental unperturbed energies for the above states were used. The energy matrices appear in Table V. The matrix element $\langle 0(+)0(-) | V | 2(+)2(-) \rangle = 3.78$ MeV is equal to the unperturbed energy difference between the states; therefore, the above-mentioned basis states are thoroughly mixed. The resulting energy spectrum appears in Fig. 7, theory B. The predicted energy spectrum is in poor agreement with experiment. The calculated quadrupole transitions of interest are: $B(E2; 2_1^+ \rightarrow 0_1^+) = 152$ e^2 F^4, and $B(E2; 0_2^+ \rightarrow 2_1^+) = 288$ e^2 F^4. All of the theoretical results are summarized in Table III. In both calculations A and B we fail to predict correctly $B(E2; 0_2^+ \rightarrow 2_1^+)$. This is due to the fact that the dominant contribution comes from $B(E2; 0_2^+(+) \rightarrow 2_1^+(+))$, which is much too large. It seems that the expanded version of the pairing-vibration model, even after mixing of the basis states is allowed, cannot explain the experimental data. The inclusion of the $0_2^+(+)$ and $0_2^+(-)$ phonons tends to improve the energy spectrum but it makes the prediction of quadrupole transitions worse.

It is difficult to understand why the above calculation A fails to reproduce the experimental quadrupole transitions. It is true, of course, that the $2_1^+(+)$ and $0_2^+(+)$ states have large deformations.[12,13] Although this was taken into account by treating the ^{42}Ca phonons phenomenologically, it is not clear to what extent the interactions can be approximated by a simple Q-Q force. Thus, one cannot confidently attribute this failure to the pairing-vibration model.

The microscopic description in conjunction with realistic interactions offers a better possibility of success provided that a detailed shell-model calculation for ^{42}Ca including deformed (e.g., 4p-2h) components becomes available. Only after such a calculation can definite conclusions about the pairing-vibration model be drawn. It is essential that this model should be able to reproduce both the energies and electromagnetic transitions simultaneously.

It is possible that one could work within the two-particle and two-hole shell-model space provided that an "effective" interaction is used that takes proper account of core deformations. In such a case the inclusion of additional two-particle and two-hole phonons will improve the situation. If, however, the inclusion of such phonons becomes necessary, the applicability of the pairing-vibration model to ^{40}Ar will be less useful, since a multiphonon description approaches a full shell-model description.

---

†Work supported in part by the National Science Foundation and the U. S. Atomic Energy Commission.

*Present address: Columbia-Greene College, Athens, New York.

‡Present address: Brookhaven National Laboratory, Upton, New York.

[1]A. Bohr, in *Proceedings of the International Symposium on Nuclear Structure, Dubna* (International Atomic Energy Agency, Vienna, Austria, 1968), p. 179.

[2]A. D. Jackson, T. T. S. Kuo, and J. D. Vergados, Phys. Letters 30B, 455 (1969).

[3]G. A. Englebertink and G. Van Middlekoop, Nucl. Phys. A138, 588 (1969).

[4]F. R. Metzger and G. K. Tandon, Phys. Rev. 148, 1133 (1966); W. J. Kossler, J. Winkler, and C. D. Kavaloski, Phys. Rev. 177, 1725 (1969).

[5]P. C. Simms, N. Benczer-Koller, and C. S. Wu, Phys. Rev. 121, 1169 (1961).

[6]P. M. Endt and C. Van der Leun, Nucl. Phys. A105, 303 (1967).

[7]W. M. Currie, L. G. Earwaker, J. Martin, and A. K. Sen Gupta, J. Phys. A 3, 73 (1970).

[8]B. D. Kern, R. W. Winters, and M. E. Jerrell, Phys. Rev. C 2, 948 (1970).

[9]R. L. Place, K. H. Buerger, Jr., T. Wakatsuki, and B. D. Kern, Phys. Rev. C 3, 2259 (1971).
[10]S. Cochavi, N. Cue, and D. B. Fossan, Phys. Rev. C 1, 1821 (1970).
[11]T. D. Newton, Phys. Rev. 78, 490 (1950).
[12]B. H. Flowers and L. D. Skouras, Nucl. Phys. A136, 353 (1969).
[13]S. Cochavi, D. B. Fossan, S. H. Henson, D. E. Alburger, and E. K. Warburton, Phys. Rev. C 2, 2241 (1970).
[14]K. Nakai, F. S. Stephens, and R. M. Diamond, Phys. Letters 34B, 389 (1971).
[15]T. T. S. Kuo and G. E. Brown, Nucl. Phys. A114, 241 (1968).

PHYSICAL REVIEW C VOLUME 5, NUMBER 3 MARCH 1972

Search for Spontaneous-Fission Isomerism in Nuclei of Medium Mass

John M. Alexander* and René Bimbot
Laboratoire de Chimie Nucléaire, Institut de Physique Nucléaire, Orsay, France
(Received 28 September 1971)

Spontaneous-fission isomers have been searched for among the recoil products from the following reactions: $Bi^{209}+H^1$, $Bi^{209}+H^2$, $Bi^{209}+He^4$, $Pb+H^2$, $Pb^{206}+He^4$, $Ir+N^{14}$, $Tm^{169}+N^{14}$, $Gd^{154}+He^4$, and $Pr^{141}+N^{14}$. The major products were $Po^{198-208}$, $Bi^{199-208}$, $Dy^{149-151}$, At, and Os. In no case have isomers been observed unambiguously. Limiting cross sections for fission isomers are $\approx 10^{-31}$ to 10^{-33} cm^2 compared to product cross sections of 10^{-24} to 10^{-25} cm^2. The limiting isomer ratios are $\approx 10^{-6}$ to 10^{-8} for decay periods of a fraction of a nanosecond to many hours. These ratios are generally less than ≈ 1 to 0.01% of the corresponding ratios for fission isomers in heavier nuclei.

1. INTRODUCTION

In recent years there has been a great deal of theoretical and experimental research on the stability of highly deformed nuclei and the role of "shell structure" for such nuclei. Experimental studies of the fission barriers by lifetime and cross-section measurements have been most useful for testing various theoretical approaches.[1] Since 1962 a number of lifetimes have been determined for spontaneous-fission isomers with neutron number greater than 126 and $Z \geq 92$.[2] Calculations by Strutinsky *et al.*[3] and by Nilsson *et al.*[4] indicate that these isomers owe their existence to a second minimum in the fission barrier which in turn arises from shell structure. These same calculations predict a certain stabilization of highly deformed nuclei with $N < 126$ and $Z > 82$ and for $N < 126$ and $Z < 82$. However, it is thought that if there are observable "shape isomers" in these nuclei of lower Z, the probability for fission should be much lower than for the spontaneous-fission isomers of $Z \geq 92$.[4] Therefore, it was very surprising when, in 1969, spontaneous-fission isomers were reported to be observed[5,6] with rather high cross sections (>1 μb) for products with $Z \approx 83$,[5] 76,[6] and 66.[5] If spontaneous fission occurs in such low-Z nuclei, one might expect that states of high angular momentum could be involved.[7]

We resolved to search for angular momentum effects on production cross sections for spontaneous fission from low-Z nuclides. The combination of the Orsay synchrocyclotron and variable-energy cyclotron provides a wide range of projectile masses and energies which in turn can provide excited nuclei with very different angular momentum spectra. For studies of Po and Bi products we have used the reactions $Bi^{209}+H^1$, $Bi^{209}+H^2$, $Pb+H^2$, $Pb^{206}+He^4$, and $Ir+N^{14}$. From the extensive cross-section studies of $Bi^{209}+H^1$ and $Pb^{206}+H^4$ we know that for the energies we used, cross sections are >100 mb for Po nuclides of $208 < A < 198$ and Bi nuclides of $208 < A < 199$.[8,9] For studies of Dy products we have used the reactions $Gd^{154}+He^4$ and $Pr^{141}+N^{14}$. Cross sections of >100 mb have also been determined in these reactions for Dy isotopes of $151 < A < 149$.[10,11]

During the course of this work, serious difficulties were reported to us in the earlier cross-section measurements for spontaneous fission of Po and Dy products.[12] It became clear that a sensitivity of much greater than one microbarn would be needed for a useful search for fission isomerism. Also, it was clear that the report[6] of delayed fission for $Z \approx 76$ should be reexamined.

The results of this study provide no positive observation of spontaneous-fission isomers with periods of a fraction of a nanosecond to many hours. The limiting cross sections are from $\approx 10^{-31}$ to 10^{-33} cm^2 and the limiting isomer ratios are $\approx 10^{-6}$